Exciton Delocalization and Superradiance in Tetracene Thin Films and Nanoaggregates

Sang-Hyun Lim,[1] Thomas G. Bjorklund,[1] Frank C. Spano,[2,*] and Christopher J. Bardeen[1,†]

[1]*Department of Chemistry, University of Illinois, 600 South Mathews Avenue, Urbana, Illinois 61801, USA*

[2]*Department of Chemistry, Temple University, Philadelphia, Pennsylvania 19122, USA*

(Received 9 September 2003; published 12 March 2004)

The structure and dynamics of luminescent excitons in tetracene thin films and nanoaggregates are investigated using time-resolved spectroscopy and theoretical calculations. The orientation of tetracene's transition dipole moment along its short molecular axis leads to properties qualitatively different from those observed in aggregates of phenylene-vinylene and thiophene oligomers, despite similar crystal structures. The spectral shape, temperature dependence, and radiative lifetime are consistent with a short-lived superradiant exciton delocalized over ~10 tetracene molecules.

DOI: 10.1103/PhysRevLett.92.107402 PACS numbers: 78.55.Kz, 42.50.Fx, 71.35.Aa, 73.61.Ph

Electronic delocalization has been studied in phenylene-vinylene [1] and thiophene conjugated oligomers [2,3], which are leading candidates for applications in organic electronics. In these molecules, the transition dipole moment μ is close to parallel to the long molecular axis. Furthermore, they aggregate in a herringbone pattern with the transition dipoles largely parallel to each other. In such cases, exciton delocalization gives rise to *H*-aggregate-type states, where the lowest exciton state is only weakly allowed by the small component of the transition dipole moment along the short molecular axis [4–6]. Such aggregates can demonstrate superradiance only if the exciton is delocalized over a large number of molecules, typically on the order of hundreds [6]. For molecules where the transition dipole moment lies *exactly* along the long molecular axis (oligothiophenes with an odd number of thiophene rings), the lowest energy exciton is strictly dipole forbidden [2]. Polyacene molecules like tetracene (structure shown in Fig. 1) differ from the phenylene-vinylenes and oligothiophenes in that the lowest dipole-allowed optical transition is polarized along the short axis of the molecule [7]. Tetracene aggregates cannot be classified as *J*- or *H*-type aggregates, since the μ's of the two molecules within the unit cell form an approximately 60° angle, distributing oscillator strength to both the bottom and the top of the exciton band. In principle, even small amounts of exciton delocalization can lead to superradiance.

In this Letter, we use experiment and theory to study emissive exciton states in polycrystalline solid tetracene. There is considerable variation concerning the shape of the absorption [8] and fluorescence [9] from solid tetracene samples, which is usually attributed to varying amounts of structural disorder. Quantitative comparison of theory and experiment is complicated by several factors, including the role of luminescent defect states and the difficulty of measuring absolute absorption and emission cross sections in solid samples. We overcome these difficulties by using picosecond time and wavelength-resolved emission spectroscopy to discriminate between excitonic and defect emission, and by using nanocrystalline colloidal particles in aqueous suspension to measure absolute quantum yields. These experiments, combined with theoretical calculations, show that the early-time emission in tetracene aggregates is due to a thermal distribution of superradiant exciton states that extend over ~10 tetracene molecules.

The tetracene used in these studies is obtained from the TCI Chemical Company and is used as received or after several recrystallizations, which did not affect the

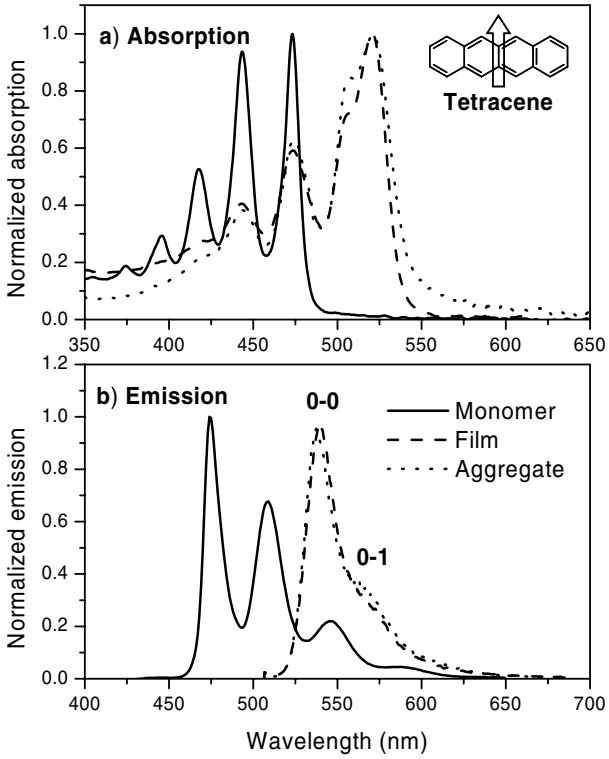

FIG. 1. (a) Absorption spectra of dilute tetracene in THF (solid line), tetracene nanoparticles in aqueous solution (dashed line), and a vacuum-deposited film of tetracene (dotted line). Also shown is the tetracene molecular structure and orientation of its transition dipole. (b) Fluorescence spectra for samples in (a). The labels 0-0 and 0-1 denote the vibronic peaks.

experimental results. Suspensions of sub-100 nm tetracene nanocrystals in water are made using a reprecipitation method [10], while tetracene thin films are made by evaporation onto a clean glass substrate under a vacuum of 10^{-6} Torr. In order to avoid self-absorption effects, the peak optical densities are kept below 0.2. Steady-state absorption and fluorescence experiments are performed using standard methods and instruments, and the fluorescence quantum yields are determined using perylene-3,4,9,10-tetracarboxylic acid as a standard [11]. The picosecond fluorescence experiments are performed under an active vacuum of $\sim 10^{-5}$ Torr in a liquid He cryostat using tunable femtosecond pulses at 40 kHz for excitation and a Hamamatsu C4334 Streakscope streak camera for detection. The streak camera data provides both time- and wavelength-resolved fluorescence data, with resolutions of 15 ps and 2.5 nm, respectively.

Figure 1 compares the steady-state absorption and fluorescence spectra of the three types of samples studied: monomeric tetracene in tetrahydrofuran (THF), ~60 nm diameter tetracene aggregates suspended in water, and a thin polycrystalline tetracene film evaporated onto a glass substrate. The aggregates and the thin solid film have similar spectral properties, including a large redshift, an upper Davydov component visible at 510 nm as a shoulder on the lowest energy absorption peak [12,13], and a significant redistribution of peak intensities within the vibronic progressions of both the absorption [Fig. 1(a)] and emission [Fig. 1(b)] spectra as compared to the monomer spectra. In Fig. 1(b), we label the emission peaks of the aggregates as 0-0 and 0-1, in analogy with the vibrational progression observed in monomeric tetracene.

Figure 2 shows fluorescence decays, integrated over all wavelengths, for a tetracene thin film at 290 and 4 K, and for the THF solution at 290 K. The tetracene thin film decays are nonexponential at all temperatures, as observed previously [14]. At 290 K one sees only the fast initial decay whose spectral shape is the same for all aggregate samples. At 4 K, the spectral snapshots at different points along the decay show distinct species which dominate the emission at different times. Given the multiple species observed in the nanosecond luminescence decay, we focus on the first 50 ps of the decay, which is most likely to reflect the intrinsic exciton properties. Our conclusions are not modified by looking at other time windows so long as they are short enough (<200 ps) to avoid significant contributions from the long-lived defect spectra. The spectrum of this early-time window is shown in Fig. 3(a) for a variety of temperatures, from 290 to 4 K. At 290 K, the 0-0 peak is enhanced relative to the lower energy 0-1 peak, when compared to the monomer spectrum. As the temperature is lowered, the 0-0 peak increases while the 0-1 peak remains constant. As the 0-0 peak becomes larger, the fluorescence quantum yield of within this 50 ps time window increases by about a factor of 2.

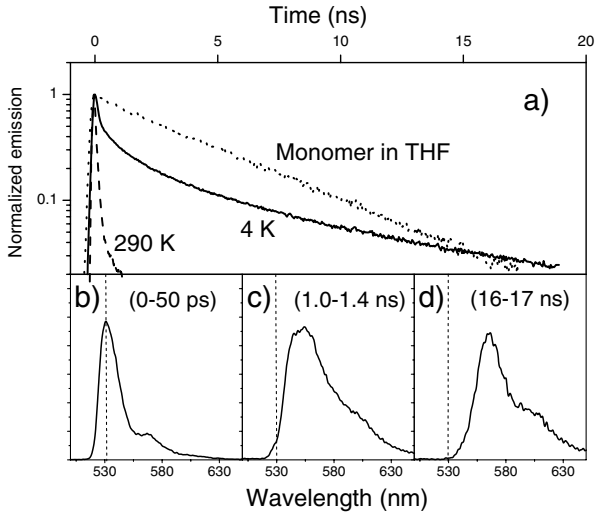

FIG. 2. (a) Fluorescence decay, integrated over all wavelengths, for dilute tetracene in THF (dotted line) and vacuum-deposited tetracene (dashed line) at 290 K, and vacuum-deposited tetracene at 4 K (solid line). The lower panels show the evolution of the fluorescence spectrum at 4 K integrated over the following time windows: (b) 0–50 ps; (c) 1.0–1.4 ns; (d) 16–17 ns.

As shown below, the vibronic line shape and its temperature dependence are sensitive measures of delocalization in a coupled exciton-phonon system. A separate measure is the enhancement of the radiative decay rate (superradiance), which should scale with N, the number of chromophores participating in the coherent exciton

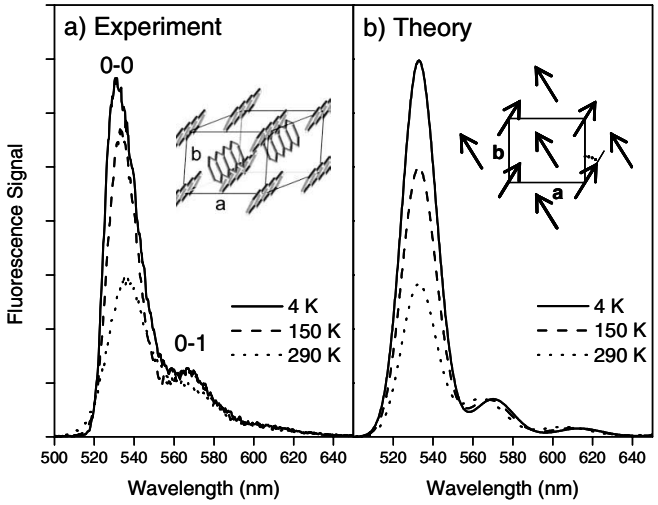

FIG. 3. (a) Experimental emission spectra of vacuum-deposited tetracene, integrated over the 0–50 ps time window, at 290, 150, and 4 K. Inset: Unit cell of tetracene crystal. (b) Theoretical emission spectra from 3×3 pinwheel calculation and Boltzmann distributions at 4, 150, and 290 K. Inset: Top view of 3×3 pinwheel aggregate used in the calculations. Arrows indicate the transition dipole moments for the b-polarized lowest energy exciton.

wave function. Measuring the fluorescence lifetime and quantum yield of the aggregate yields its radiative lifetime, proportional to μ^2:

$$k_{\mathrm{rad}} = \frac{1}{\tau_{\mathrm{rad}}} = \frac{\phi_{\mathrm{fl}}}{\tau_{\mathrm{fl}}} = \frac{64\pi^4 n \bar{\nu}^3}{3h}\,\mu_{\mathrm{em}}^2, \tag{1}$$

where n is the refractive index of the medium, $\bar{\nu}$ is the frequency of emission, and h is Planck's constant. For monomeric tetracene in the THF solution, we obtain a fluorescence decay time of 4.6 ns and a quantum yield of 0.17, which leads to a radiative lifetime of 27.1 ns, in good agreement with literature values ranging from 27 to 32 ns [15,16]. To measure the room temperature quantum yield of the tetracene aggregates, we use the water-suspended nanoaggregates in the same setup as for tetracene in solution. Our justification for equating the colloidal and thin film samples rests on the equivalence of their room temperature absorption and emission spectra, fluorescence decay times, and the fact that when the nanoparticles are deposited onto a substrate their temperature dependent luminescence is indistinguishable from that of the evaporated film. The fluorescence quantum yield is 0.008, while the decay is biexponential with times of 82 ps (coefficient of 0.947) and 350 ps (coefficient of 0.064). The fluorescence spectrum is constant over the course of the decay, indicating that the decay is due to a single species. If we define the average fluorescence lifetime as

$$\begin{aligned}\langle \tau_{\mathrm{fl}} \rangle &= \int_0^\infty dt\, N_{\mathrm{ex}}(t) = \int_0^\infty dt (A e^{-t/T_1} + B e^{-1/T_2}) \\ &= AT_1 + BT_2, \end{aligned} \tag{2}$$

and use Eq. (1), we find the radiative lifetime to be 12.5 ± 2 ns, smaller by a factor of 2.1 than that of the tetracene molecule in solution. If we assume that the biexponential decay is due to two different types of species, we would obtain an even shorter radiative lifetime, 8.5 ns, for the major species. The decrease in radiative lifetime for aggregated tetracene relative to monomeric tetracene provides concrete evidence of superradiance, although exciton fission and other luminescence quenching processes lead to a lower overall quantum yield in the solid.

The experimental data can be modeled by assuming an exciton-phonon system confined to a finite number of tetracene molecules. We analyze the Hamiltonian [17,18]

$$\begin{aligned} H = {} & \omega_0 \sum_n b_n^\dagger b_n + \omega_0 \lambda \sum_n (b_n^\dagger + b_n) |n\rangle\langle n| \\ & + \sum_{m,n} J_{mn} |m\rangle\langle n| + \omega_M + \lambda^2 \omega_0, \end{aligned} \tag{3}$$

where $b_n^\dagger$ (b_n) is the creation (destruction) operator for an intramolecular vibration on molecule n with frequency ω_0. Linear exciton-phonon coupling is established through the Huang-Rhys factor, λ^2. We set $\omega_0 = 1400\ \mathrm{cm}^{-1}$ and $\lambda^2 = 1$ in order to reproduce the main features of the monomer absorption spectrum in Fig. 1(a). The electronic state, $|n\rangle$, indicates that the molecule at n is in the electronically excited state with 0-0 transition frequency ω_M while all others remain in their ground states. Resonant energy transfer between molecules at m and n is determined by the excitonic coupling coefficient, J_{mn}.

Neglecting interlayer interactions, we consider two-dimensional arrays of tetracene molecules in their crystalline orientations. We obtain eigenstates (dressed excitons) and energies under the two-particle approximation [19–21] and subsequently input these quantities into an expression for the emission spectrum. We studied model aggregates built up from the basic four-molecule (2×2) pinwheel structure and included only nearest (edge-to-face) excitonic interactions, J_0. A value of $J_0 = 280\ \mathrm{cm}^{-1}$ was selected, as it reproduces the $650\ \mathrm{cm}^{-1}$ 0-0 Davydov splitting in a 4×4 aggregate (which is near the experimental crystal value). In order to obtain the temperature dependence we assumed emission from a Boltzmann distribution of low energy excitons. Hence, at $T = 0$ only the lowest energy exciton contributes to the emission spectrum. At this temperature, one can show that the 0-0 emission rate, $I^{0\text{-}0}$, scales as $I^{0\text{-}0} \propto NF\cos^2\phi$, where N is generally the number of coherently emitting molecules, F is a generalized Franck-Condon factor [20–23], and ϕ is the herringbone angle shown in the inset of Fig. 3(b). By contrast, the replica intensities are relatively insensitive to the exciton coherence size, N, as was shown also for the case of distyrylbenzene (DSB) and oligothiophene aggregates at $T = 0$ [20–23].

Figure 3(b) shows the calculated temperature dependent spectra for a 3×3 aggregate. The calculation explains why the amplitude of the 0-0 line changes with temperature but the 0-1 line does not. Since wave vector selection rules dictate that the 0-0 line arises from only the lowest exciton state (and not from thermally activated excitons), the 0-0 intensity is most sensitive to changes in the exciton coherence volume due to thermal scattering into other exciton states, and it alone diminishes with increasing temperature. In contrast, the replica emission lines are nearly independent of temperature, consistent with their presence in the emission spectra from all the states in the exciton band. Hence, the increase in the 0-0 emission while the 0-1 emission remains constant is a clear signature of decreasing dynamic disorder, which leads to greater coherence lengths. A more detailed treatment of the temperature dependence can be found elsewhere [23]. Note that in this treatment the radiative decay rate scales as N only at $T = 0$; at finite temperatures the radiative rate is reduced due to dynamic scattering [23,24]. Figure 4 plots the temperature dependence of the ratio of the aggregate-to-monomer radiative rates. The theoretical curves are calculated using 2×2, 3×3, and 4×4 arrays of tetracene molecules. The experimental values are determined by taking the experimental

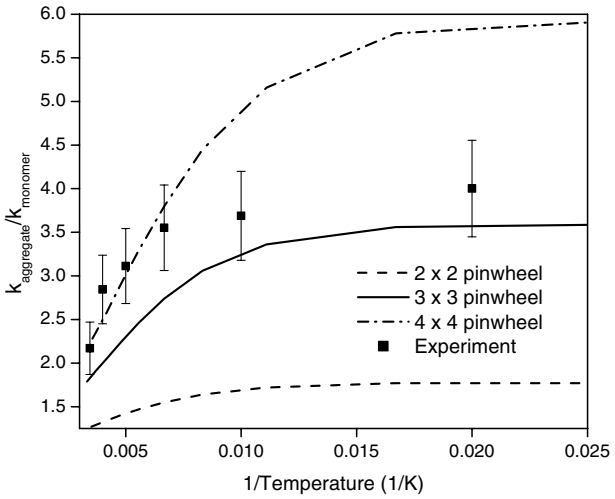

FIG. 4. Temperature dependence of the ratio of radiative rates, $k_{\text{aggregate}}/k_{\text{monomer}}$ from theoretical calculations for 2×2 (dashed line), 3×3 (solid line), and 4×4 (dot-dashed line) pinwheels, along with experimental values obtained by multiplying the ratio measured at 290 K by the relative increase in integrated fluorescence within the 0–50 ps time window. The error bars are due to uncertainty in the 290 K radiative rate measurement.

ratio of 2.1 determined at room temperature and scaling it by the relative increase in the 0–50 ps emission at the lower temperatures. This assumes that the quantum yield increase is due only to an increased radiative rate, i.e., that any change in the fast nonradiative rate for the exciton is negligible. The data are plotted as a function of $1/T$ since this clearly shows the leveling-off behavior at low temperatures due to the shift of the Boltzmann distribution into the lowest exciton state. The 3×3 aggregate gives the best agreement overall with our experimental spectra and radiative rates, allowing us to estimate the early-time ($\sim$50 ps) coherence size of the exciton to be approximately ten molecules in these disordered films. Improvements in the theoretical analysis, such as including additional vibrational modes, inhomogeneous site energies, and taking into account the nonequivalence of the tetracene molecules in the unit cell of the crystal, may change this estimate slightly.

Previous theoretical work on DSB and quaterthiophene (OT4) has shown how the interplay of excitonic and vibronic coupling affects the absorption and emission spectra [21–23]. Similar effects occur in tetracene, where the in-plane constructive interference, discussed for DSB and OT4 in terms of the small short axis component of μ, is now possible for the entire μ, allowing for superradiance in tetracene *without a threshold*. The experimental results and theoretical analysis are both consistent with the existence of a superradiant exciton delocalized over $\sim$10 molecules.

We acknowledge funding from NSF Grants No. CHE-99-84683 (C. J. B.) and No. DMR-0305173 (F. C. S.) and the Sloan Research Foundation (C. J. B.).

*Email address: bardeen@uiuc.edu
†Email address: spano@astro.temple.edu

[1] D. Oelkrug, A. Tompert, H.-J. Egelhaaf, M. Hanack, E. Steinhuber, M. Hohloch, H. Meier, and U. Stalmach, Synth. Met. **83**, 231 (1996).
[2] F. Meinardi, M. Cerminara, A. Sassella, A. Borghesi, P. Sperman, G. Bongiovanni, A. Mura, and R. Tubino, Phys. Rev. Lett. **89**, 157403 (2002).
[3] R. Osterbacka, C. P. An, X. M. Jiang, and Z. V. Vardeny, Science **287**, 839 (2000).
[4] M. Kasha, H. R. Rawls, and M. A. El-Bayoumi, Pure Appl. Chem. **11**, 371 (1965).
[5] D. Beljonne, J. Cornil, R. Silbey, P. Millie, and J. L. Bredas, J. Chem. Phys. **112**, 4749 (2000).
[6] F. C. Spano, Chem. Phys. Lett. **331**, 7 (2000).
[7] H. B. Klevens and J. R. Platt, J. Chem. Phys. **17**, 470 (1949).
[8] R. Hesse, W. Hofberger, and H. Bassler, Chem. Phys. **49**, 201 (1980).
[9] G. Peter and H. Bassler, Chem. Phys. **49**, 9 (1980).
[10] H. Y. Kim, T. G. Bjorklund, S.-H. Lim, and C. J. Bardeen, Langmuir **19**, 3941 (2003).
[11] H. Langhals, J. Karolin, and L. B.-A. Johansson, J. Chem. Soc., Faraday Trans. **94**, 2919 (1998).
[12] J. Tanaka, Bull. Chem. Soc. Jpn. **38**, 86 (1965).
[13] D. W. Schlosser and M. R. Philpott, Chem. Phys. **49**, 181 (1980).
[14] A. Wappelt, A. Bergmann, A. Napiwotzki, H. J. Eichler, H. J. Jupner, A. Kummrow, A. Lau, and S. Woggon, J. Appl. Phys. **78**, 5192 (1995).
[15] S. L. Murov, I. Carmichael, and G. L. Hug, *Handbook of Photochemistry* (Marcel Dekker, Inc., New York, 1993), 2nd ed.
[16] C. Burgdorff, S. Ehrhardt, and H.-G. Lohmannsroben, J. Phys. Chem. **95**, 4246 (1991).
[17] A. Witkowski and W. Moffitt, J. Chem. Phys. **33**, 872 (1960).
[18] P. O. J. Scherer and S. F. Fischer, Chem. Phys. **86**, 269 (1984).
[19] M. R. Philpott, J. Chem. Phys. **55**, 2039 (1971).
[20] F. C. Spano, J. Chem. Phys. **116**, 5877 (2002).
[21] F. C. Spano, J. Chem. Phys. **118**, 981 (2003).
[22] X. H. Sun, Z. Zhao, F. C. Spano, D. Beljonne, J. Cornil, Z. Shuai, and J.-L. Bredas, Adv. Mater. **15**, 818 (2003).
[23] F. C. Spano, J. Chem. Phys. (to be published).
[24] F. C. Spano, J. R. Kuklinski, and S. Mukamel, Phys. Rev. Lett. **65**, 211 (1990).